Geoderma 361 (2020) 114090

Contents lists available at ScienceDirect

Geoderma

journal homepage: www.elsevier.com/locate/geoderma

Durable and ductile double-network material for dust control

Chiao-Yueh Lo[a], Hamed Khodadadi Tirkolaei[b], Mutian Hua[a], Igor M. De Rosa[a,c], Larry Carlson[c], Edward Kavazanjian Jr.[b], Ximin He[a,*]

[a] Department of Materials Science and Engineering, Henry Samueli School of Engineering and Applied Science, University of California, Los Angeles, 410 Westwood Plaza, Los Angeles, CA 90095, United States
[b] Center for Bio-mediated and Bio-inspired Geotechnics, Arizona State University, 650 E. Tyler Mall, Tempe, AZ 85281, United States
[c] Institute for Technology Advancement, Henry Samueli School of Engineering and Applied Science, University of California, Los Angeles, Engineering VI, Suite 510, Los Angeles, CA 90095, United States

ARTICLE INFO

Handling Editor: Yvan Capowiez

ABSTRACT

Dust generation is a world-wide issue due to its serious deleterious effects on the environment, human health and safety, and the economy. Although various dust suppression methods have been used for decades, some critical drawbacks in state-of-the-art technology still remain unsolved, such as short-lasting, ground water impact, and prone to water. This work reports a soil stabilizer based on non-toxic material and forms a ductile and durable double-network in soil, namely "D^3 soil stabilizer", which not only improves soil mechanical toughness of surface soil but also suppresses dust generation. A copolymer comprising hydrophilic and hydrophobic components combined with enzyme-induced carbonate precipitation is utilized as an in-situ gelation binder to soil particle. The tunable hydrophobic-to-hydrophilic component ratio minimizes undesirable soil matrix expansion and mechanical strength loss upon experiencing wet-dry processes, while still retains good water affinity. We further demonstrated controllable treatment depth by fine-tuning precursor composition, which is essential to minimize environmental impact. The double-network morphology with carbonate precipitate embedded uniformly in polymer matrix is observed via microscopic imaging. The nature of outstanding ductility, high durability against water, and good long-term stability were supported by systematic unconfined compressive strength (UCS) measurements on treated soil, which show strong inter-particles binding, good retention of peak strength, increased strain at peak strength, and increased toughness after soil samples have experienced wet-dry processes.

1. Introduction

Dust generation is a world-wide issue due to its serious deleterious effects on the environment, human health and safety, and the economy. Dust refers to the wind-blown particles eroded by air. The soil particles with the size of around 0.18 mm (*i.e.* fine sand) was reported to have the highest susceptibility to air erosion (Garrels, 1951). Very fine soil particles are more resistant to detachment by wind due to inter-particle cohesion (Wilson et al., 2001). Dust particles can contaminate water and food and, when inhaled, can lead to serious respiratory ailments, while dust clouds are traffic hazards as they can reduce visibility during road and aircraft transportation. The concentration of airborne fugitive dust particles is used as an air quality indicator by the United State Environmental Protection Agency (EPA). Sources of airborne fugitive dust include construction activities, travel on unpaved roads, wind storms, wildfires, and agricultural activities.

The conventional method for mitigating dust is to spray water on the source area, while the main issue with applying water is that the dust is suppressed only as long as the source area remains wet, and it is often complicated by the scarcity of water in hot, arid areas, making procurement of sufficient water difficult and costly. Incorporation of hygroscopic salts such as magnesium or calcium chloride in water applied for dust control is often done in an attempt to retain moisture on the surface. However, application of salt has many disadvantages, including to the need for relatively high concentration of salt and associated equipment corrosion and surface and ground water impacts (due to the high solubility of the salts in water). Various types of chemical dust suppressants including surfactants, polymers, bituminous products, and resins (Foley et al., 1996), are also commercially available.

Notwithstanding that there is a wide variety of soil stabilizing materials that facilitates soil strengthening and dust suppression, there is a need for alternatives with enhanced effectiveness and less

* Corresponding author.
E-mail address: ximinhe@ucla.edu (X. He).

https://doi.org/10.1016/j.geoderma.2019.114090
Received 16 July 2019; Received in revised form 13 November 2019; Accepted 14 November 2019
0016-7061/ Published by Elsevier B.V.

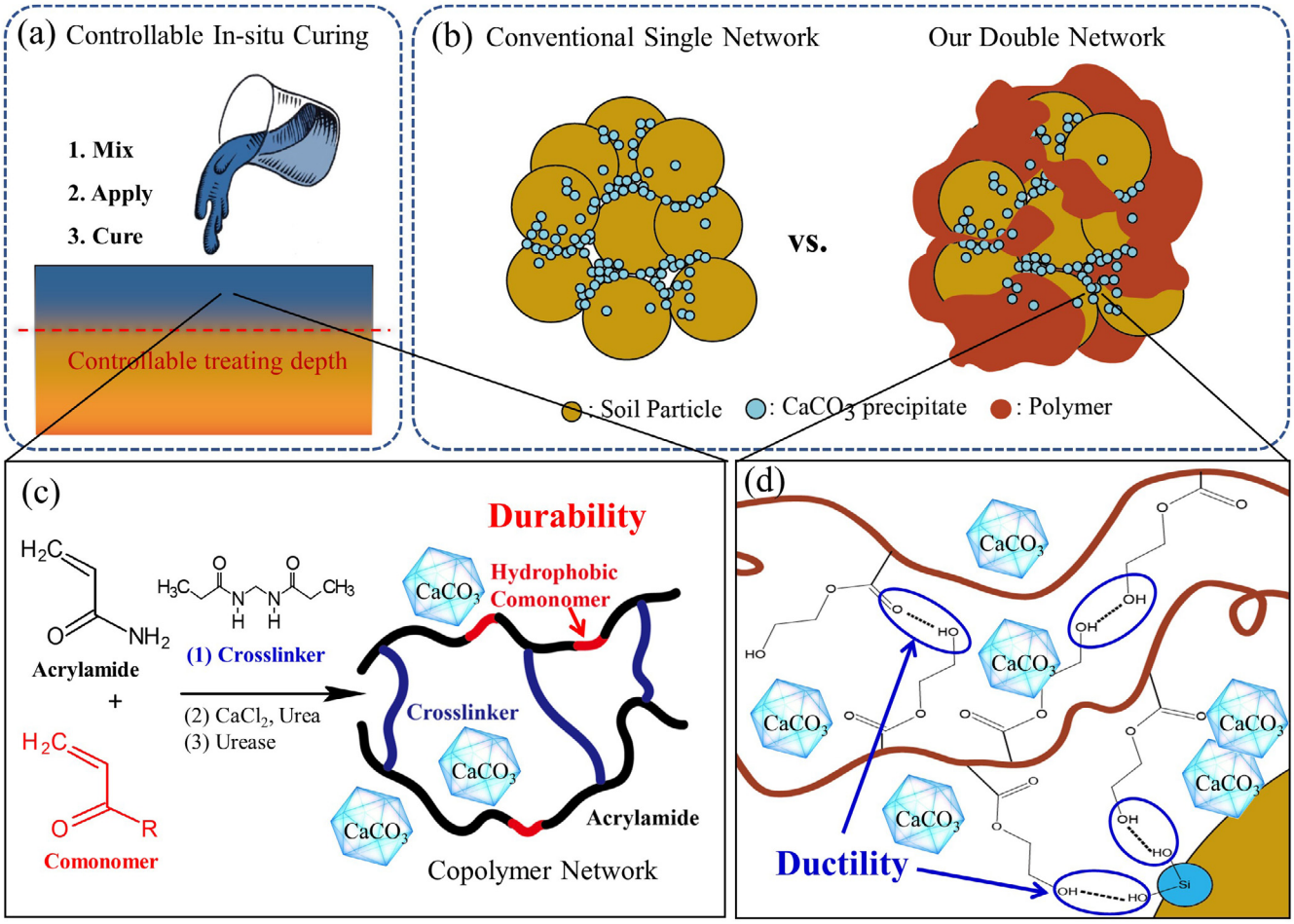

Fig. 1. Design concept of the durable and ductile double-network (D^3) dust suppressant: (a) in-situ curing of liquid-form agent of D^3 dust suppressant with tunable curing time results in controllable treatment depth, (b) improved binding ability with carbonate-polymer double network. Rationally designed copolymerization achieves (c) improved water durability with reduced polymer swelling and (d) good ductility with reversible intermolecular hydrogen bonds (shown in dashed lines).

environmental impact. Within last two decades, extensive attention has been paid to use of biocompatible and bio-based products for dust suppression, including synthetic hydrogels, bio-polymers, and biologically mediated mineral precipitation (Bang et al., 2009; Chen et al., 2015; Hamdan and Kavazanjian, 2016; Kavazanjian et al., 2009; Liu et al., 2018; Meyer et al., 2011). Synthetic hydrogels and bio-polymers are attractive because of their water retaining ability and because their application typically does not require compaction (Chang et al., 2015c), which make them compatible with establishment of vegetation on the treated surface. Biopolymers such as gellan gum, guar gum (Chang et al., 2015b) and xanthan gum (Chang et al., 2015a; Chang et al., 2015c) can provide not only a surficial soil strength level comparable to cement-treated soil but also high ductility via reversible hydrogen bonding (Chang et al., 2015b). However, water-soluble biopolymers lose strength and can be flushed from the soil when they are exposed to water. By contrast, synthetic hydrogels are cross-linked hydrophilic polymers and thus water insoluble. In fact, synthetic polymers have been used as a soil conditioner in agriculture for decades due to their good water retention and anti-erosion functions (Barvenik, 1994; Mirzababaei et al., 2017; Orts et al., 2007; Paganyas, 1975).

Moreover, cohesionless soils are also lower in load-bearing capacity, shear strength, and plasticity which make them prone to damage during earthquake (e.g., liquefaction) and in heavy rainy season. Some traditional soil strengthening methods such as geosynthetics matting and cementation, which produces poly(carbonate-silicones) to bind soil particles and significantly improve soil strength (Firoozi et al., 2017), suffer from bio-incompatible issues, as the formed dense water-blocking layer suppresses plant root system development and causes severe surface water runoff (Eith and Koerner, 1992; Federation and Engineers, 1998; Koerner, 2012). These new challenges in environmental protection and infrastructure sustainability bring up growing demands for new soil strengthening techniques that are non-toxic, long lasting, and effective in enhancing ground loading capacity and resiliency.

Recently, innovative biologically mediated mineral precipitation techniques, such as microbially induced carbonate precipitation (MICP) and enzyme induced carbonate precipitation (EICP) have been proposed for dust control (Bang et al., 2009; Hamdan and Kavazanjian, 2016; Meyer et al., 2011). These techniques bind soil particles together via precipitation of carbonates as cementitious agent, forming an erosion resistant crust on the treated surface to mitigate dust generation. MICP and EICP combined with hydrogels have been shown to facilitate the retention of the treatment solution at the surface, enhancing erosion-resistant crust formation (Hamdan et al., 2016; Wang, xxxx).

We have previously reported synthesis of a hybrid soil stabilizing material based on a combination of EICP and a biopolymer, xanthan gum (Hamdan et al., 2016), or a synthetic hydrogel, poly(acrylic acid) (PAAc) (Zhao et al., 2016). This method can significantly enhance the strength of treated soil after dehydrated (Hamdan et al., 2016; Zhao et al., 2016). However, this approach suffers from a water durability problem arose from drastic polymer swelling.

In this research, we managed to mitigate the water durability problems using a series of hydrophilic-hydrophobic copolymers instead of hydrogels. Additionally, we used a non-toxic (Andersen, 2005; Berndt

et al., 1991; Horak et al., 1997) polyacrylamide (PAAm) backbone to replace the polyacrylic acid (PAAc) backbone used in previous research (Zhao et al., 2016) to facilitate curing under ambient temperature conditions instead of at elevated temperature and for reducing peroxide initiator usage. The curing rate was also improved from longer than 1 day to several minutes (under ambient temperature). This new soil stabilizing material provides the ability to control solidification of the polymer precursor fluid, which results in a controllable and tunable treatment depth (*i.e.* crust thickness) and minimizes the potential for pollution to ground water. This material is also more ductile than our earlier formulations, reducing the chance of crack formation in the surface crust under traffic loads. Furthermore, it does not exacerbate CO_2 emissions and exhibits good water affinity for vegetation growth.

The rational design concept of durable, ductile double-network (D^3) soil stabilizer is shown in Fig. 1. Specifically, to improve the "water durability" of treated soil, tunable hydrophilicity is achieved by molecular-level design using a copolymer composed of both hydrophilic and hydrophobic units. The overall hydrophobicity of the copolymer network is determined and tuned by the "backbone: co-monomer" ratio. With more hydrophobic units, the water binding ability within polymer is weaker, so the undesirable swelling which is usually observed in hydrogels can be reduced.

To mitigate fracture in the treated surface due to deformation caused by human activity and traffic, we employ a "double-network" design that utilizes milli-/micro-scale polymer network to reinforce the inorganic-cemented soil network with "ductility", inspired from microfiber reinforcement of concretes, where polymer microfibers provide ductility in concrete matrix and sandy soil (Durairaj and Janaki Sundaram, 2015; Liu et al., 2017). These treatments are proven to be capable of transforming matrix bulk characteristics from brittle to malleable, which provide impact dissipation ability and prevent crack or fracture upon external strain. With these micron-scale fiber-based network, peak strength and strain at fracture of reinforced soil are improved (Liu et al., 2017). Therefore, we anticipated polymer network to mechanically hold soil particles in place and leads to higher fracture toughness.

On the other hand, EICP and MICP have been demonstrated to be effective for binding cohesionless soil particles (Hamdan and Kavazanjian, 2016; Kavazanjian et al., 2017; Meyer et al., 2011; Mujah et al., 2017) by providing cementation at the inter-particle contacts but results in a relatively brittle structure. Here, we combined an EICP-based inorganic crystal network with the above-described copolymer-based organic network to both bind soil particles and create ductility. By selecting polymers capable of forming resilient, dynamic intermolecular bonding, including the hydrogen bond between polymer chains and between polymer and soil particles (shown in Fig. 1(d) as dashed lines) as well as increased anchoring points on soil particle surface, a higher toughness of treated soil can be achieved via increased bulk "ductility". In addition, both the copolymer network and the EICP treatment can be applied from aqueous solution at ambient temperature. This common merit facilitates an *in-situ* curing process that can trap stabilizer solution at ground surface and provide precise control of the solution penetration into soil, mitigating any potential for contamination of ground water.

2. Materials and methods

2.1. Materials

F60 silica sand was provided by US Silica. Acrylamide (AAm, 98%, extra pure), (hydroxyethyl)methacrylate (HEMA, 97%, stabilized), acrylic acid (AAc, 98%, extra pure, stabilized), ammonium persulfate (APS, 98%, ACS grade), tetramethylethylenediamine (TEMED), calcium chloride (96%, extra pure), and urea (bioreagent grade) were purchased from Fisher Scientifics and used as received without further purification. Urease from jack beans, *Canavalia ensiformis*, (reported activity of 34,960 units/g), and N,N′-methylenebisacrylamide (BIS, 99%) were purchased from Sigma Aldrich and used as received.

2.2. Instrument

Scanning electron microscopy (SEM) images and energy dispersive X-ray spectroscopy (EDS) samples were first sputtered with ~5 nm thickness of gold, and then examined in NOVA NanoSEM 230, under low vacuum (~50 Pa) condition. Unconfined compressive dtress tests were conducted in a "GCTS Testing Systems" and "Instron 5966 universal testing machine". Powder X-ray diffraction (XRD) spectra of soil samples were obtained using Cu-Kα radiation on a Panalytical X'Pert Pro Powder X-ray Diffractometer.

2.3. Preparation of D^3 stabilization precursor solutions

(1) For preparing the D^3 stabilization precursor solution of poly (AAm-co-HEMA)-EICP as depicted in Fig. 1(c), a 4 g mixture of AAm and HEMA (70:30 M ratio), 0.2 g of BIS as crosslinker, and 25 μL of TEMED as catalyst were dissolved in 10 mL of distilled water. Then, this polymer precursor solution was mixed with the EICP precursor solution, a mixture of $CaCl_2$ (1.25 M), urea (1.875 M), and free urease enzyme (jack bean urease = 4.5 mg/mL) in a 5:4:1 vol ratio. Last, to initiate the polymerization, APS as initiator was added to the mixture at 0.5% w/w ratio with respect to the total polymer concentration. (2) To prepare the two control agents, polyacrylamide (PAAm)-EICP precursor and polyacrlic acid (PAAc)-EICP precursor, the AAm and HEMA mixture was replaced by respectively 4 g of AAm or 4 g of AAc (added dropwisely), with other components kept the same.

2.4. Preparation of soil samples for unconfined compressive strength (UCS) tests and SEM inspection

Unconfined compressive strength (UCS) was performed to evaluate inter-particle bond strength in the treated samples, which indicates how strong the treated sample is against erosion. To achieve uniform soil columns for UCS, the precursor solution was mixed with the soil. Ottawa F-60 sand (with the specifications presented in Table 1) was used in this study as it has particle size that has been reported to be highly susceptible to air erosion (Garrels, 1951). 180 g of F-60 sand was thoroughly mixed with 50 mL of precursor solution. Then, the mixture was poured into a cylindrical plastic mold with an inner diameter of 1 3/4″. Relative density of the soil was around 40%. Air bubbles were removed carefully by gently stirring the mixture within the plastic mold, followed by sufficient settlement of sand particles. Then, the samples were cured at ambient temperature for 5–30 min (depending on precursor composition) until the samples were solidified. After the curing, the soil sample was extracted from the mold and then oven-

Table 1
Specifications of F-60 sand.

Silica Content	D_{10} (mm)	D_{30} (mm)	D_{50} (mm)	D_{60} (mm)	e_{max}	e_{min}	G_s	Hydraulic conductivity at D_r = 40% (cm/s)
99.7	0.15	0.19	0.23	0.26	0.83	0.60	2.65	0.022

dried for 48 h at 50 °C. The purpose of oven-drying is to accelerates the drying process, and since it is applied after gelation, which is the characteristic phenomena indicating polymerization completion, the oven-drying has negligible impact on the polymerization reaction. Each sample was approximately 4.00 cm in diameter and 7.60 cm in height. After oven drying, each sample was subject to UCS testing at a strain rate of 1.27 mm/min. A small piece of each sample was also used for SEM examination. The sample was placed on the SEM sample holder by carbon tape and then sputter-coated with a 5 nm-layer of gold to prevent charging of the material by the electron beams.

2.5. Powder XRD analysis

Powder XRD specimens were prepared by collecting the supernatant during soil sample molding, followed by precursor gelation, dried overnight in oven to form clear-white granules, and carefully ground into white powder with ceramic mortar. The powder was placed in rectangular sample holders for examination, and the resulting spectrum were analyzed by built-in database on Panalytical X'Pert Pro Powder X-ray Diffractometer.

2.6. Treatment depth examination

We have examined the treatment solution infiltration depth as well as the thickness of crust formed on the treated surface. Precursor solutions with different initiator concentrations were applied to the top surfaces of the untreated soil sample columns and the infiltration depth was measured. The precursor solutions were allowed to infiltrate into soil by gravity and the solution infiltration depth was traced by the progression of wet-dry interface. The samples were allowed to cure under the 25 °C ambient condition for 5–30 min (depending on precursor composition) and then the soil samples were placed into an oven at 50 °C for 48 h to remove residual water. Afterwards, the non-bound soil was removed carefully from the bottom of each soil sample and the thickness of surface crust was recorded as actual treatment depth.

2.7. Water infiltration test

A water infiltration test was conducted on dried treated soil samples using a lab-scale method modified from the single-ring infiltrometer method (ASTM International, 2018; Johnson, 1963) sometimes used in the field. A transparent test tube with graduation marks was placed in the center of each sample before curing. Then, the samples were prepared using the same protocol as for UCS tests. To measure the water infiltration rate, distilled water was added into the tube to a certain height above the sample's surface and the cumulative volume of water infiltrated into soil was calculated by measuring the reduction in height of the water column above the soil surface. The infiltrated volume was plotted versus elapsed time. The infiltration rates increased with time and eventually reached a maximum value. The saturated infiltration rate (*i.e.* slope of linear part on the plot) was taken as the hydrated water infiltration rate. The infiltration rates between samples with and without hydrophobic monomer HEMA, *i.e.*, soil samples treated by PAAm-EICP and P(AAm-co-HEMA)-EICP, were compared.

2.8. Wet-dry cycle durability tests

To evaluate bond strength under cycles of wetting and drying and swelling under wet condition in the treated samples, the completely dried soil samples (treated with the same amount of stabilizer precursor solutions, 50 mL per 180 g of F-60 sand) were first immersed in distilled water for 8 h to remove precursor residual and achieve equilibrium swollen volume. Next, the wet samples were again oven-dried for 48 h at 50 °C. The UCS test was conducted on these samples and stress-strain curves as well as toughness were obtained. Volumes of bare polymers and soil samples after 1–3 wetting and drying cycles were directly measured by their dimensions with a digital vernier scale at 0.01 mm precision. The results were compared with those samples which were not subject to wetting and drying cycles. The volume of each sample after wetting to the volume of the same sample at dry condition was defined as swelling ratio.

2.9. Long-term heat durability

To evaluate the long-term durability of the samples, we employed the accelerated thermal degradation test described in our previous work (Zhao et al., 2016). In this test, small-scale poly(PAAm-co-30% HEMA)-treated cylindrical soil samples (2.50 cm × 1.85 cm) were placed in an oven under 50 °C for 30 days. By applying kinetic equations of chemical reactions (*i.e.*, Arrhenius relationships, $lnk = lnA - \frac{E_a}{R}\frac{1}{T}$, in which the logarithm of reaction rate constant k is linearly related to the reciprocal of reaction temperature T), it was estimated that this accelerated thermal degradation condition is equivalent to more than 3 months exposure under 25 °C. After the 30-days of exposure at 50 °C, the strength of the samples was determined using UCS testing. The change in strength and toughness before and after the heat exposure is reported as an indication of long-term thermal durability.

3. Results and discussion

3.1. Evidence of soil particle binding

Under SEM examination, we observed that the copolymer materials used in this study have good affinity with sandy soil particles surface. As Fig. 2(a) shows, the soil particles are surrounded and bonded tightly by cured polymer. Fig. 2(b) shows the calcium carbonate precipitates formed from EICP reaction, observed as spheres with 1–2 μm diameter. The chemical composition of each microstructures observed in SEM were further confirmed by EDS mapping. In Fig. 2(d), three representative elements, namely carbon, silicon, and calcium, were selected to mark polymer region, soil particle region, and calcite region, respectively. The EDS mapping result showed that soil particles (silicon-rich region) were surrounded by polymer network (carbon-rich region), while the universally existing calcium may indicate calcium carbonate precipitates embedded within polymer and on soil particle surfaces or calcium ion trapped within polymer network, as depicted in Fig. 2(c).

To further confirm the existence of calcium carbonate precipitates, powder XRD was conducted, and the spectrum shown in Fig. 2(e) was taken on supernatant retrieved while molding the sand samples. The supernatant was solidified by polymer network, dried, and ground into powder, and this powder contains a poly(AAm-co-HEMA) matrix embedding both calcite and suspended sand particles. The diffraction peaks noted indicate a significant amount of quartz, which is the main component of F60 sand, while the characteristic peak at $2\theta = 29^{\circ}$ indicated the existence of calcium carbonate in rhombohedral calcite form. The broad hill at small angle region is originated from the amorphous poly(AAm-co-HEMA) matrix. It is reported that precipitation of calcium carbonate on soil particle surface can improve the mechanical properties of bulk soil with increased cohesion between soil particles (Kavazanjian et al., 2009; Meyer et al., 2011; Mujah et al., 2017). Also, researches focusing on composite materials showed that nanoscale mineral precipitates, such as calcium carbonate, calcium phosphate, as well as clay particles within polymer network, enhanced the mechanical properties of the matrix (Rauner et al., 2014; Rauner et al., 2017; Schexnailder and Schmidt, 2009; Thoniyot et al., 2015). In such system, these mineral particles can physically strengthen the matrix as filler (Rai and Singh, 2004) or forms reversible non-covalent bonding (Gao et al., 2015), which contributes to strength and toughness.

In addition, uniformly distributed calcium overlapping the polymer region in EDS mapping in Fig. 2(d) could also indicate the metal complex formed between calcium ion and the metal-chelating amide

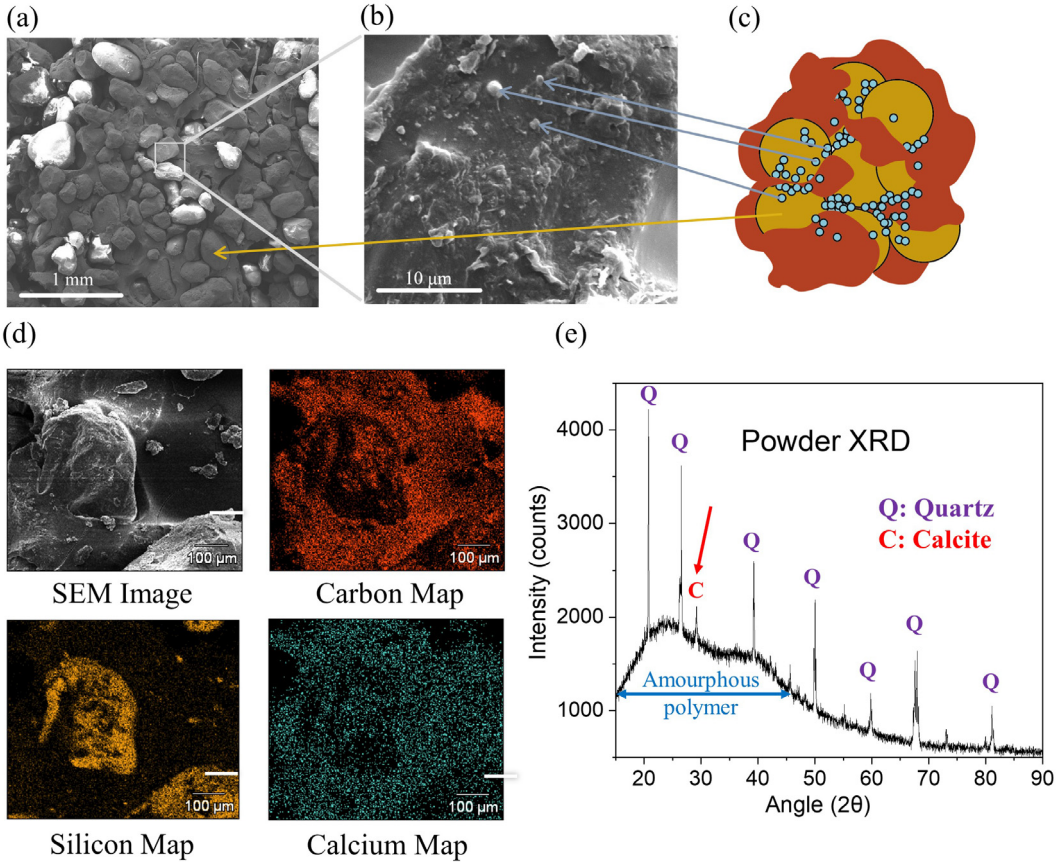

Fig. 2. SEM images showing microstructure of (a) treated soil particle, reinforced by polymer network and (b) calcium precipitate. (c) Conceptual image depicting distribution of each composition. (d) The conceptual image in (c) is based on our observation from EDS mapping of carbon, silicon and calcium. (e) Powder XRD spectrum of supernatent showing characteristic peaks of calcium carbonate in rhombohedral calcite form at 2θ = 29° (symbolled with C). The broad hill is originated from the amorphous polymer, and the rest of peaks (symbolled with Q) are originated from quartz.

groups (–NH_2) within polyacrylamide. These calcium chelating sites were also reported to function as reversible, non-covalent crosslinking, which contributes to the ductility, toughness and the ability to recover from deformation of composite network (Li et al., 2014; Sun et al., 2012; Yuk et al., 2016). Therefore, we believe that the microstructure characteristic we observed contributes to its enhanced mechanical properties, which will be discussed in latter sections.

3.2. Evidence of bond strength

To address the efficacy of the binder material for creating enough inter-particle cohesion to resist against wind erosion, UCS test on the treated sand columns was used as an indication of inter-particle bond strength. A higher UCS represents a greater inter-particle cohesion, which means a higher velocity of eroding agent (*i.e.*, wind) is required to cause particles detachment. In addition, the UCS shows how resistant the surface is against fracture due to the loads caused by human activity and traffic on the surface. As shown in Table 2, UCS of the treated specimens ranges between 1.7 MPa and 5.4 MPa, which is comparable with pavement materials (Bondietti et al., 2004). This demonstrates that all these materials have the potential of application for surficial treatment of low volume unpaved roads and construction sites which are two of the main sources of dust generation.

3.3. Treatment depth control

Controlling the thickness of the crust on the surface and preventing the treatment solution to run-off or penetrate deep into ground water are essential factors that should be considered in soil surface treatment for dust control. To demonstrate the potential for precise control of treatment depth, we have achieved different solution infiltration rate by altering the reaction rate of precursor solution with different initiator concentrations, as shown in Fig. 3(a). Here, the precursor solution was applied to soil sample by pouring onto the top surface of soil column, and the progression of precursor infiltration front can be traced by the movement of interface between wet soil and dry soil. PAAm-EICP precursor solutions with initiator to total polymer weight ratio of 0.25%, 0.50%, and 1.00% resulted in increasing curing speed and thus decreasing precursor infiltration depths from > 12.0 cm to 10.0 cm and 6.0 cm, respectively. However, the final treatment depth is a result of the competition between curing speed and infiltration speed. In Fig. 3(b), a slower curing rate of 30 min (with 0.25% initiator) results in more solution runoff and dilution of reactive agents. The incomplete polymerization led to less dense, crumbled structure of bound soil and relatively shallower treatment depth of only 6.5 cm (left), in contrast with its > 12 cm infiltration depth. Meanwhile, those treated with 0.50% (middle) and 1.00% initiator (right) resulted in final treatment depths of 8.5 cm (10.0 cm infiltration) and 6.0 cm (6.0 cm infiltration), showing more effective solidification within their infiltration depths. The shallowest surface treatment depth with the most densely bound soil (right) was achieved with the rapist curing rate of 3 min, in which curing occurred before the precursor could infiltrate deep into the soil. The deepest treatment depth (middle) was achieved with medium curing rate of 10 min, in which the curing rate and precursor solution infiltration rate were more optimally coupled. We also observed that the precursor solutions are initially capable of infiltrating quickly into soil due to their low viscosity. Then, the solution infiltration slowed down due to viscosity increase as the polymerization took place and

Table 2
Mechanical properties of soil samples treated with PAAm-EICP and P(AAm-co-HEMA)-EICP with different HEMA ratios showed robust mechanical behavior in contrast with PAAc-EICP treatment. After wet and redried, these samples also showed significantly improved retainment of mechanical properties, comparing to the disastrous loss in PAAc-EICP treated soil.

	Original		Wet-redried	
	Peak Strength (kPa)	Strain at Peak Strength (%)	Peak Strength (kPa)	Strain at Peak Strength (%)
PAAc	1755	8.98	1917	1.79
PAAm	5419	3.89	5205	7.46
P(AAm-co-10% HEMA)	4743	3.61	5498	5.56
P(AAm-co-20% HEMA)	4255	3.46	4201	4.53
P(AAm-co-30% HEMA)	3498	2.67	3557	4.16
P(AAm-co-40% HEMA)	3992	3.34	4167	4.24

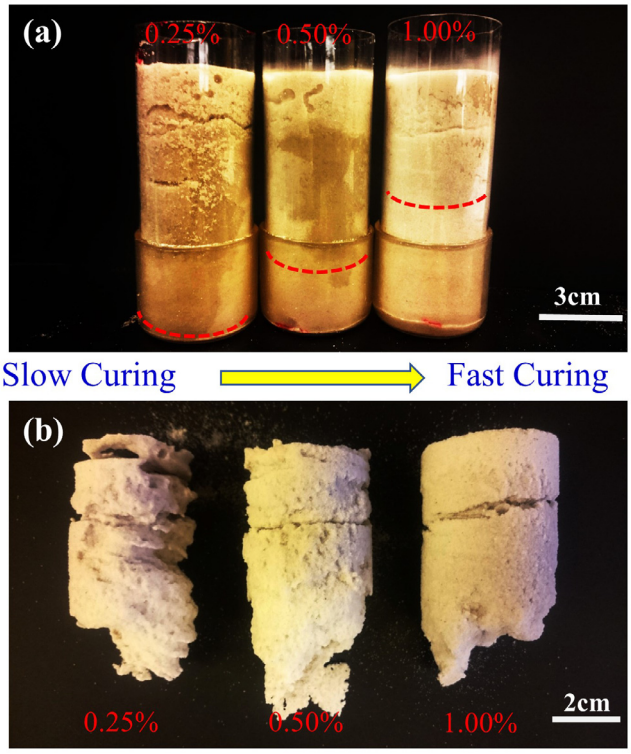

Fig. 3. Soil samples treated with slower hardening (far-left) to faster hardening (far-right). (a) shows different, controllable solution-infiltration depth and (b) shows the actual treatment depth.

eventually solidified when the reaction completed. Therefore, with the tunability and flexibility in reaction speed of our method, the infiltration rate can be accelerated or decelerated to adapt into soil with different permeability. Our solutions can also be tailored for various soil condition and applications, such as surface and ground treatment. Furthermore, this high controllability of solidification is a crucial property of our method to avoid chemical pollution and unnecessary disturbance to surroundings.

3.4. Durability: water affinity and stability

We proposed a copolymer composed of both hydrophilic and hydrophobic units with tunable hydrophilicity in aim of improving "water durability" of treated soil. However, our preliminary results revealed that surfactants in the polymer precursor solution, which are essential in mediating the copolymerization reaction of hydrophilic acrylamide with hydrophobic units, significantly lower the reactivity and increase the viscosity of the precursor solution. As a result, the presence of surfactant in the precursor solution causes severe difficulties in practical application. Thus, we selected a co-monomer that is less hydrophilic than the backbone AAm monomer but still with acceptable solubility in water, namely (hydroxyethyl)methacrylate (HEMA), to fabricate poly(AAm-co-HEMA) in this research. The highly bio-compatible polyHEMA derivatives have long been used as contact lens material in many ophthalmic applications, owing to their malleability when wet and robustness when dried (Childs et al., 2016). Use of HEMA monomer as a property modifier to improve the fracture strength of acrylic and methacrylic hydrogels has also been reported (Omidian et al., 2010).

We aimed to reduce swelling behavior of our soil stabilization treatment during wet-dry cycles, while still retaining good vegetation compatibility. As shown in Fig. 4(a), the initial water infiltration rate of the dried poly(AAm-co-HEMA)-EICP treated soil is increased, reflecting a higher water affinity. The hydrated infiltration rate (linear part) of soil samples also increased to 0.472 (cm/hour) when treated by poly (AAm-co-HEMA) in contrast with 0.123 (cm/hour) of PAAm. The faster hydrated infiltration rate may indicate a higher porosity or good water affinity of treated soil, both properties are essential for vegetation root system development (Hamza and Anderson, 2002; Hamza and Anderson, 2003; Hamza and Anderson, 2005). Thus, an improved vegetation compatibility can be achieved with poly(AAm-co-HEMA) owing to good water retention nature of hydrogels and good porosity, comparing to low vegetation compatibility from compacted, water-blocking layer of traditional cement and inorganic soil stabilizers.

For swelling behavior characterization, poly(AAm-co-HEMA)-EICP treated soil showed swelling ratio reduction. Bare poly(AAm-co-HEMA) copolymers with increasing HEMA content showed reduction in swelling ratio from 760% to 500% (w/w), as depicted in Fig. 4(b), which is critical for reducing soil structure damage upon wet-dry cycles. As a result, in Fig. 4(c), soil samples treated with the less-swelling poly (AAm-co-HEMA) also showed a significant volumetric swelling reduction, in which the swelling ratios are reduced to approximately 0%. Furthermore, this beneficial effect on soil crumble prevention also applied to multiple wet-dry cycles. PAAc-EICP as well as PAAm-EICP treated soil samples not only showed higher volumetric swelling ratios, but also an increased swelling with more wet-dry cycles. This phenomenon can be attributed to the repeated swelling of polymer, which enlarges the pores within soil samples and provide extra spacing for even more severe polymer swelling. In comparison, swelling ratio of poly(AAm-co-HEMA)-EICP treated soil remained at negligible level, leading to significantly enhanced water durability.

We also traced the changes in mechanical properties and micromorphologies when soil samples were exposed to multiple wet-dry cycles, and the results indicated that modification with hydrophobic comonomer successfully improved water durability of treatment. In Fig. 5(a), the macroscopic appearances of soil samples after wet-dry showed that samples treated with PAAm-EICP and poly(AAm-co-HEMA)-EICP have smoother surfaces with less visible micro-pores and are thus less crumbled after wet-redried comparing to previously reported PAAc-EICP treatment. We further examined the SEM images of soil samples treated by poly(AAm-co-HEMA)-EICP before and after up

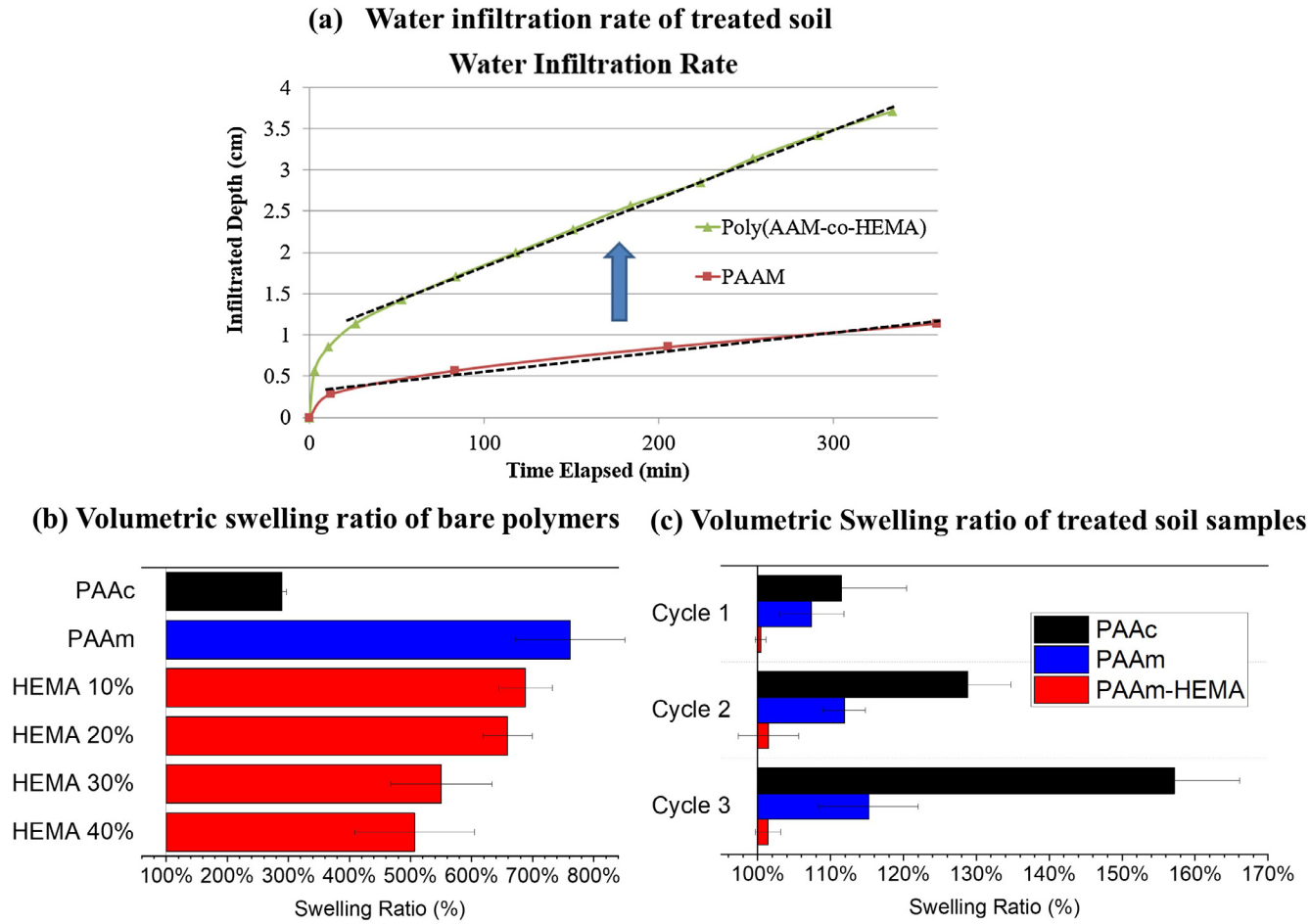

Fig. 4. (a) Water infiltration rate conducted on soil samples treated with PAAm-EICP (red line) and poly(AAm-co-HEMA)-EICP (green line). (b) Swelling ratio (w/w) of poly(AAm-co-HEMA) copolymers are reduced with higher HEMA content. (c) Volumetric swelling behavior of PAAc-EICP treated samples become worse after multiple wet-dry cycles, while poly(AAm-co-HEMA)-EICP treated samples remain nearly un-swollen. (For interpretation of the references to colour in this figure legend, the reader is referred to the web version of this article.)

to 3 wet-dry cycles, as shown in Fig. 5(b). There is little change in micro-morphology after multiple wet-dry cycles, indicating that inter-particle binding by double network remained intact even after multiple wet-dry cycles.

To sum up, according to better vegetation compatibility, less volumetric change upon wetted, and stable microstructure after wet-dry cycles, we have proved that incorporation of poly(AAm-co-HEMA) is a more suitable soil stabilization choice under wet condition than both PAAc and PAAm.

3.5. *Durability: Strength loss after wetting and drying cycles*

To evaluate the improvement in water durability, we compared the mechanical performance via unconfined compressive strength (UCS) tests before and after rewetting the soil samples treated by PAAm-EICP derivatives and previously reported PAAc-EICP stabilizers for comparison. The averaged peak strengths and corresponding strains are shown in Table 2, and the representative stress-strain curves are shown in Fig. 6. The zigzag fluctuations in stress-strain curves was observed in the brittle samples when detachment of sand particles and small chunks at the edges of the samples occurred during compressive loading before the whole sample fails. Before rewetting, for the freshly made and dried samples, all PAAm-EICP derivatives treated soil showed a more robust behavior comparing to PAAc-EICP treated samples, with 200%–250% of strength enhancement, while sacrificing 60% of the maximum strain and ~25% of elastic modulus.

In Fig. 7, to compare the mechanical performance before and after wet-dry, the peak strength, strain at peak strength, and toughness of the samples after one wet-dry cycle and freshly prepared were recorded accordingly. The ratio of each property after wet-dry to freshly prepared were then calculated and compared. As shown in Fig. 7 (b), after wet and redried, samples treated with PAAc-EICP lost 80% of deformability (strain at peak strength) and exhibited highly brittle mechanical behavior; by contrast, samples treated with PAAm-EICP and P(AAm-co-HEMA)-EICP increased in ductility and deformability. Loss of deformability indicated a significant loss of adhesion between polymer network and soil particles, which caused by the enormous polymer volume change upon water-induced swelling and shrinkage. Therefore, by introducing PAAm and HEMA with less swelling behavior as the organic network, we effectively retained the ductility and the peak strength of the treated soil after wet-dry cycle. These results and explanation are verified by their macroscopic structures in Fig. 5. PAAc-EICP treated soil became porous (Fig. 5 (a)) from polymer swelling and this resulted in crumbled structure after wet-dry cycle; by contrast, PAAm-EICP treated samples remain intact as revealed by the microstructures shown in Fig. 5(b–d). This improvement can be attributed to the non-charged nature of PAAm in water, which effectively reduced the swelling, compared to the negatively charged PAAc with high swelling ratio. Hence, with the high ductility well retained or even increased due to minimized loss of organic network adhesion, PAAm and its copolymers are more water-durable choices in the organic-inorganic double-network stabilizer than PAAc. Furthermore, the peak strengths and the

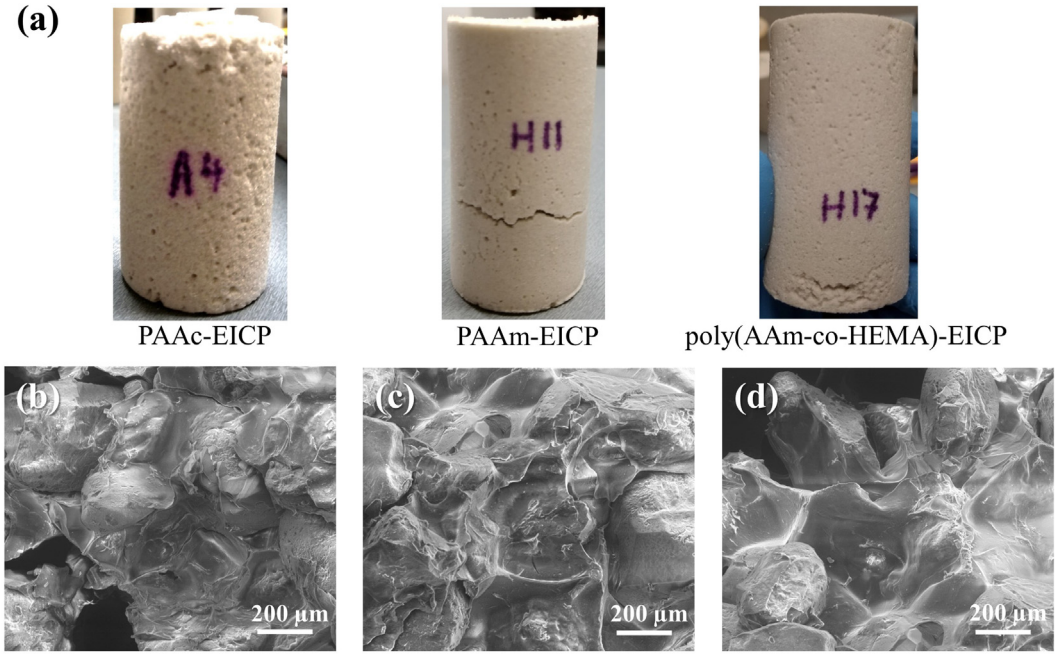

Fig. 5. (a) Appearance of soil samples treated with PAAc-EICP, PAAm-EICP and poly(AAm-co-HEMA)-EICP. The numerous visible pores on PAAc-EICP and PAAm-EICP treated samples are caused by polymer swelling. SEM images of poly(AAm-co-HEMA)-EICP treated soil samples (b) before wet-dry cycles, (c) after 1 cycle, and (d) after 3 cycles. Little degradation of these binding networks occurred.

respective strains of these sandy soil samples treated by ~5 wt% of our copolymers and EICP reaction lie at ~4000 kPa and ~3%, respectively. This reported method has achieved significantly improved mechanical performance, especially more ductile and resilient than the state-of-the-art polymeric fiber reinforcement (Ilieş et al., 2017; Liu et al., 2017; Oncu and Bilsel, 2017) or treatments using inorganic or organic single-network stabilizer alone (Chang et al., 2016; Chang et al., 2015a; Choi et al., 2017).

Among the poly(AAm-co-HEMA)-EICP treated samples, we also observed that the peak strength of samples treated with PAAm-EICP was well maintained, and those treated with poly(AAm-co-HEMA) effectively improved by 5–16% (Fig. 7 (a)). With increasing HEMA:AAm ratio, the treated soil sample become more robust but less deformable. Thus, copolymerization of HEMA with AAm also allows for fine-tuning between robustness and ductility by varying the HEMA:AAm ratio. This good tunability and customizability make our modular-designed copolymers more flexible to fit various applications.

3.6. Ductility: toughness

To evaluate impact-damping ability, we also calculated the toughness of treated soil samples by integrating the area below stress-strain curves before peak strength, and compare the results before and after samples were wet and redried. In Fig. 8, after one wet-dry cycle, samples treated with PAAc-EICP lost over 80% of its original toughness, while samples treated with PAAm-EICP and poly(HEMA-co-HEMA)-EICP showed increased toughness up to 229% of the original value. To sum up, soil stabilizer utilizing both PAAm-EICP and poly(AAm-co-HEMA)-EICP are superior to PAAc-EICP in terms of better sustainability of both mechanical strength and overall energy-damping capability (*i.e.*, toughness), which lead to dramatically improved water resistance and durability especially in wet condition.

By comparing the toughness of samples with different HEMA contents, we also observed that incorporating more HEMA co-monomer within poly(HEMA-co-HEMA) causes decrease in soil sample overall toughness as well as smaller toughness improvement after wet-dry cycle. Therefore, to balance the overall toughness and water durability, an optimum HEMA:AAm ratio can be found at around 10%. Summarizing the toughness data with peak strength, strain at peak strength and elastic modulus in previous section, the incorporation of HEMA in the PAAm-EICP stabilizer makes the treated dry soil more rigid and strong, owing to polyHEMA's rigid nature, as the hydrophobic methyl side on polyHEMA turns outward around its central carbon under dry condition.

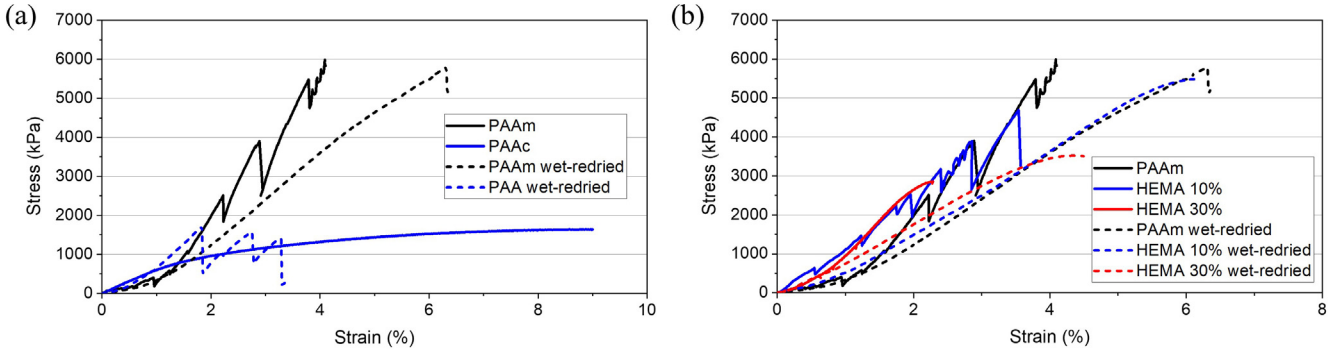

Fig. 6. The UCS stress-strain curves of (a) PAAc-EICP and PAAm-EICP treated samples, and (b) PAAm-EICP and poly(AAm-co-HEMA)-EICP treated samples.

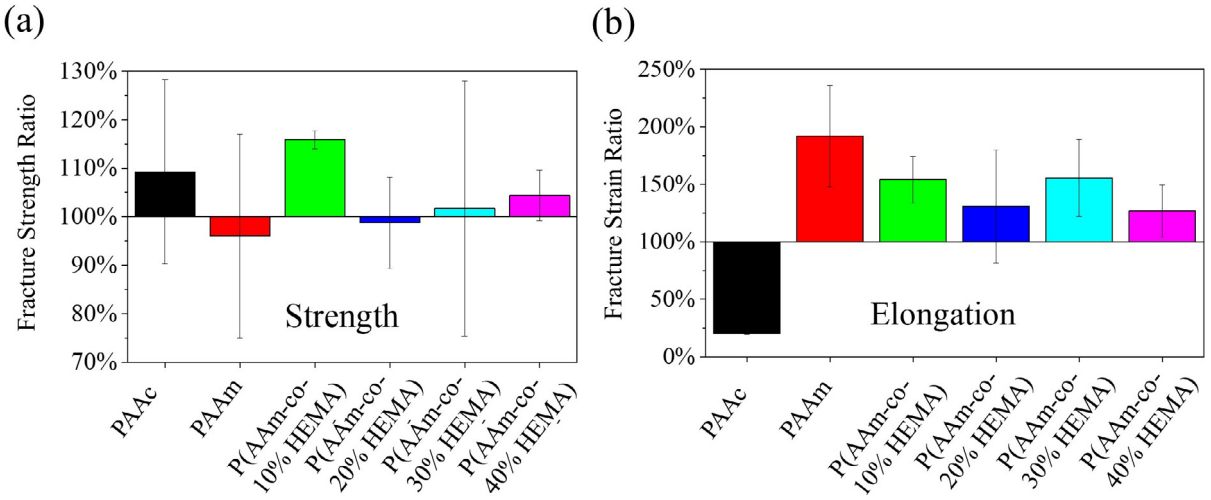

Fig. 7. Comparison of (a) fracture strength and (b) strain at fracture before and after wet-dry process. The ratios are taken as the mechanical properties after wet-dried over their original values. The deformability can be retained when incorporating PAAm and poly(AAm-co-HEMA) copolymers. Characteristics also varies with different HEMA:AAm ratio.

(a)

Properties / Samples	Original	Rewet-redried	Change
	Toughness (J/m³)	Toughness (J/m³)	%
P(AAm-co-10% HEMA)	115150.30	14235.70	12.36%
P(AAm-co-20% HEMA)	85582.34	170904.80	199.70%
P(AAm-co-30% HEMA)	62751.64	143812.50	229.18%
P(AAm-co-40% HEMA)	68364.55	97182.19	142.15%
P(AAm-co-10% HEMA)	46591.83	78918.29	169.38%
P(AAm-co-20% HEMA)	61134.05	81345.21	133.06%

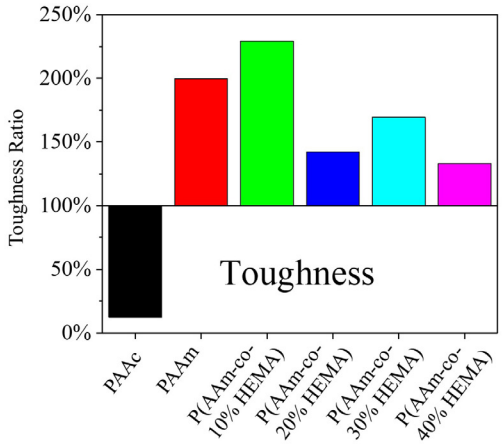

Fig. 8. Toughness of soil samples treated with (a) different recipes and their respective change after wet-dry process, and (b) bar chart comparing the toughness change of all samples. Samples treated with PAAc-EICP lost over 80% of its original toughness, while samples treated with PAAm-EICP and poly(AAm-co-HEMA)-EICP showed increased toughness.

3.7. Long-term heat durability

Since the dust problem is mainly occur in arid area, for practical application, it is crucial to keep the polymer networks intact during exposure to ambient heat. As shown in Fig. 9, all mechanical properties of poly(AAm-co-30% HEMA) treated samples slightly increased after 30 days of thermal exposure at 50 °C, which possibly arose from continuous hardening of polymer under elevated temperature. This indicated good long-term thermal durability in terms of mechanical strength.

4. Conclusions

In summary, we have achieved our design concept of the "D^3 soil stabilizer", which features high ductility and durability via organic-inorganic double-network, by replacing traditional hydrogel with poly (AAm-co-HEMA) copolymers. These exceptional properties were verified by analyzing the observations and quantitative data from SEM image, EDS and powder XRD spectrum, UCS tests, wet-dry cycle degradation tests, and long-term thermal stability tests. These results proved this design to be effective in significantly improving the ductility, toughness and water-durability of current stabilization method with high cohesion strength for dust suppression. We have also demonstrated the ability of precise and tunable solidification, as well as the flexibility of tuning soil physical properties by varying copolymer composition. These extra benefits accompanied with excellent water-durability enable our treatment method to be utilized in situations where pollutant erosion into the drain should be avoided and impact to surroundings should be controlled, such as drainage basin and mine tailings, to prevent soil erosion, and minimized stabilizer loss, and being adaptive to broader environmental conditions.

Declaration of Competing Interest

The authors declare that they have no known competing financial interests or personal relationships that could have appeared to influence the work reported in this paper.

Acknowledgments

This work was supported by the National Science Foundation under grant CMMI-1742759 and grant CMMI-1233658. The authors are

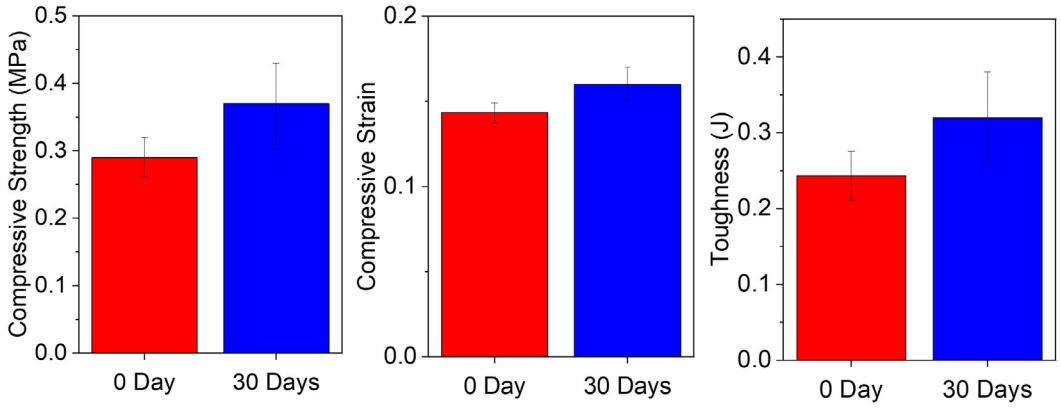

Fig. 9. Long term stability test: the mechanical properties of poly(AAm-co-30% HEMA) treated soil after 30 days under 50 °C well maintained even with slight increase.

grateful for the NSF support. Any opinions or positions expressed in this paper are the opinions and positions of the authors only, and do not reflect any opinions or positions of the NSF.

References

Andersen, F.A., 2005. Amended final report on the safety assessment of polyacrylamide and acrylamide residues in cosmetics. Int. J. Toxicol. 24, 21–50.

ASTM International, W.C., PA, 2018. ASTM D3385-18 Standard Test Method for Infiltration Rate of Soils in Field Using Double-Ring Infiltrometer.

Bang, S.S., Bang, S., Frutiger , S., Nehl , L.M., and Comes , B.L., 2009. Application of Novel Biological Technique in Dust Suppression, Transportation Research Board 88th Annual Meeting, Washington DC, United States, pp. 0831.

Barvenik, F.W., 1994. Polyacrylamide characteristics related to soil applications. Soil Sci. 158 (4), 235–243.

Berndt, W.O., Bergfeld, W.F., Boutwell, R.K., Carlton, W.W., Hoffmann, D.K., Schroeter, A.L., Shank, R.C., 1991. Final report on the safety assessment of polyacrylamide. J. Am. College Toxicol. 10 (1), 193–203.

Bondietti, M., Murphy, D., Jenkins, K., Burger, R., 2004. Research on the stabilisation of two different materials using bitumen emulsion and cement, Proceedings of the 8th Conference on Asphalt Pavements for Southern Africa (CAPSA'04). Citeseer, pp. 16.

Chang, I., Im, J., Cho, G.C., 2016. Introduction of microbial biopolymers in soil treatment for future environmentally-friendly and sustainable geotechnical engineering. Sustainability 8 (3).

Chang, I., Im, J., Prasidhi, A.K., Cho, G.C., 2015a. Effects of Xanthan gum biopolymer on soil strengthening. Constr. Build. Mater. 74, 65–72.

Chang, I., Prasidhi, A.K., Im, J., Cho, G.C., 2015b. Soil strengthening using thermo-gelation biopolymers. Constr. Build. Mater. 77, 430–438.

Chang, I., Prasidhi, A.K., Im, J., Shin, H.D., Cho, G.C., 2015c. Soil treatment using microbial biopolymers for anti-desertification purposes. Geoderma 253, 39–47.

Chen, R., Lee, I., Zhang, L.Y., 2015. Biopolymer stabilization of mine tailings for dust control. J. Geotech. Geoenviron. Eng. 141 (2).

Childs, A., Li, H., Lewittes, D.M., Dong, B., Liu, W., Shu, X., Sun, C., Zhang, H.F., 2016. Fabricating customized hydrogel contact lens. Sci. Rep. 6.

Choi, S.G., Chu, J., Brown, R.C., Wang, K., Wen, Z., 2017. Sustainable biocement production via microbially induced calcium carbonate precipitation: use of limestone and acetic acid derived from pyrolysis of lignocellulosic biomass (vol 5, pg 5183, 2017). ACS Sustainable Chem. Eng. 5 (8) 7449 7449.

Durairaj, S., Janaki Sundaram, S., 2015. Shear improvement in soft soil using fiber in a random manner. J. Chem. Pharm. Sci. 8 (4), 798–800.

Eith, A.W., Koerner, R.M., 1992. Field-evaluation of geonet flow-rate (transmissivity) under increasing load. Geotext. Geomembr. 11 (4–6), 489–501.

Federation, W.E., Engineers, A.S.C., 1998. Urban Runoff Quality Management. WEF.

Firoozi, A.A., Olgun, C.G., Baghini, M.S., 2017. Fundamentals of soil stabilization. Int. J. Geo-Eng. 8 (1).

Foley, G., Cropley, S., Giummarra, G., Ltd, A.T.R., 1996. Road Dust Control Techniques: Evaluation of Chemical Dust Suppressants' Performance. ARRB Transport Research Limited.

Gao, G.R., Du, G.L., Sun, Y.N., Fu, J., 2015. Self-healable, tough, and ultrastretchable nano-composite hydrogels based on reversible polyacrylamide/montmorillonite adsorption. ACS Appl. Mater. Interfaces 7 (8), 5029–5037.

Garrels, R.M., 1951. A Textbook of Geology. Harper.

Hamdan, N., Kavazanjian Jr., E., 2016. Enzyme-induced carbonate mineral precipitation for fugitive dust control. Geotechnique 66 (7), 546–555.

Hamdan, N., Zhao, Z., Mujica, M., Kavazanjian, E., He, X.M., 2016. Hydrogel-assisted enzyme-induced carbonate mineral precipitation. J. Mater. Civ. Eng. 28 (10).

Hamza, M.A., Anderson, W.K., 2002. Improving soil physical fertility and crop yield on a clay soil in Western Australia. Aust. J. Agric. Res. 53 (5), 615–620.

Hamza, M.A., Anderson, W.K., 2003. Responses of soil properties and grain yields to deep ripping and gypsum application in a compacted loamy sand soil contrasted with a sandy clay loam soil in Western Australia. Aust. J. Agric. Res. 54 (3), 273–282.

Hamza, M.A., Anderson, W.K., 2005. Soil compaction in cropping systems – a review of the nature, causes and possible solutions. Soil Tillage Res. 82 (2), 121–145.

Horak, D., Cervinka, M., Puza, V., 1997. Hydrogels in endovascular embolization.6. Toxicity tests of poly(2-hydroxyethyl methacrylate) particles on cell cultures. Biomaterials 18 (20), 1355–1359.

Ilies, N.M., Circu, A.P., Nagy, A.C., Ciubotaru, V.C., Kisfaludi-Bak, Z., 2017. Comparative Study on Soil Stabilization with Polyethylene Waste Materials and Binders. 10th International Conference Interdisciplinarity in Engineering, Inter-Eng 2016 181, 444–451.

Johnson, A.I., 1963. A field method for measurement of infiltration. 1544F.

Kavazanjian, E., Jr., Almajed, A., Hamdan, N., 2017. Bio-Inspired Soil Improvement Using EICP Soil Columns and Soil Nails. Grouting 2017: Grouting, Drilling, and Verification (288), 13–22.

Kavazanjian Jr, E., Iglesias, E., Karatas, I., 2009. Biopolymer soil stabilization for wind erosion control.

Koerner, R.M., 2012. Designing with Geosynthetics, sixth ed. Xlibris US.

Li, J.Y., Illeperuma, W.B.K., Suo, Z.G., Vlassak, J.J., 2014. Hybrid hydrogels with extremely high stiffness and toughness. ACS Macro Lett. 3 (6), 520–523.

Liu, J., Feng, Q., Wang, Y., Bai, Y.X., Wei, J.H., Song, Z.Z., 2017. The effect of polymer-fiber stabilization on the unconfined compressive strength and shear strength of sand. Adv. Mater. Sci. Eng.

Liu, Y., Nie, W., Jin, H., Ma, H., Hua, Y., Cai, P., Wei, W., 2018. Solidifying dust suppressant based on modified chitosan and experimental study on its dust suppression performance. Adsorpt. Sci. Technol. 36 (1–2), 640–654.

Meyer, F.D., Bang, S., Min, S., Stetler, L., S. Bang, S., 2011. Microbiologically-Induced Soil Stabilization: Application of Sporosarcina pasteurii for Fugitive Dust Control, 2011.

Mirzababaei, M., Arulrajah, A., Ouston, M., 2017. Polymers for stabilization of soft clay soils. Proceedings of the International Scientific Conference Transportation Geotechnics and Geoecology (Tgg-2017) 189, 25–32.

Mujah, D., Shahin, M.A., Cheng, L., 2017. State-of-the-art review of biocementation by microbially induced calcite precipitation (MICP) for soil stabilization. Geomicrobiol. J. 34 (6), 524–537.

Omidian, H., Park, K., Kandalam, U., Rocca, J.G., 2010. Swelling and mechanical properties of modified HEMA-based superporous hydrogels. J. Bioactive Compatible Polymers 25 (5), 483–497.

Oncu, S., Bilsel, H., 2017. Influence of polymeric fiber reinforcement on strength properties of sand-stabilized expansive soil. Polymer-Plastics Technol. Eng. 56 (4), 391–399.

Orts, W.J., Roa-Espinosa, A., Sojka, R.E., Glenn, G.M., Imam, S.H., Erlacher, K., Pedersen, J.S., 2007. Use of synthetic polymers and biopolymers for soil stabilization in agricultural, construction, and military applications. J. Mater. Civ. Eng. 19 (1), 58–66.

Paganyas, K.P., 1975. Results of the use of series k compounds for the control of irrigational soil erosion. Soviet Soil Sci. 7 (5), 591–598.

Rai, U.S., Singh, R.K., 2004. Synthesis and mechanical characterization of polymer-matrix composites containing calcium carbonate/white cement filler. Mater. Lett. 58 (1–2), 235–240.

Rauner, N., Meuris, M., Dech, S., Godde, J., Tiller, J.C., 2014. Urease-induced calcification of segmented polymer hydrogels – a step towards artificial biomineralization. Acta Biomater. 10 (9), 3942–3951.

Rauner, N., Meuris, M., Zoric, M., Tiller, J.C., 2017. Enzymatic mineralization generates ultrastiff and tough hydrogels with tunable mechanics. Nature 543 (7645), 407-+.

Schexnailder, P., Schmidt, G., 2009. Nanocomposite polymer hydrogels. Colloid Polym. Sci. 287 (1), 1–11.

Sun, J.Y., Zhao, X.H., Illeperuma, W.R.K., Chaudhuri, O., Oh, K.H., Mooney, D.J., Vlassak, J.J., Suo, Z.G., 2012. Highly stretchable and tough hydrogels. Nature 489 (7414), 133–136.

Thoniyot, P., Tan, M.J., Karim, A.A., Young, D.J., Loh, X.J., 2015. Nanoparticle-hydrogel composites: concept, design, and applications of these promising, multi-functional materials. Adv. Sci. 2 (1–2).

Wang, X., Polymer-Modified Microbially Induced Carbonate Precipitation Treatment Method for Surface Erosion Prevention.

Wilson, R.G., Smith, J.A., Miller, S.D., Fornstrom, K.J., 2001. Sugarbeet Production Guide. University of Nebraska-Lincoln.

Yuk, H., Zhang, T., Parada, G.A., Liu, X.Y., Zhao, X.H., 2016. Skin-inspired hydrogel-elastomer hybrids with robust interfaces and functional microstructures. Nat. Commun. 7.

Zhao, Z., Hamdan, N., Shen, L., Nan, H.G., Almajed, A., Kavazanjian, E., He, X.M., 2016. Biomimetic hydrogel composites for soil stabilization and contaminant mitigation. Environ. Sci. Technol. 50 (22), 12401–12410.